Metal Nanoparticle Deposition for TOF-SIMS Signal Enhancement of Polymers

Abigale Marcus and Nicholas Winograd*

Department of Chemistry, The Pennsylvania State University, 104 Chemistry Building, University Park, Pennsylvania 16802

A novel technique for improved time-of-flight secondary ion mass spectra of polymer ions is presented. This technique is a simple preparatory method, which involves deposition of a submonolayer coverage of metal nanoparticles on the surface of a polymer sample enabling an overall increase in characteristic polymer ions. This procedure gives spectra with enhanced intensity, a larger number of characteristic polymer peaks, and peaks of higher mass. Both Au and Ag nanoparticles were employed to facilitate the ionization of the polymer characteristic secondary ions. Moreover, these experiments demonstrate that the nanoparticles allow localization of high-mass fragment ions during imaging experiments utilizing focused ion beams. In general, we show that the metal nanoparticle deposition method is effective for time-of-flight secondary ion mass spectrometry examination of polymers.

Time-of-flight secondary ion mass spectrometry (TOF-SIMS) is a powerful tool for analysis of chemical, biological, and polymer surfaces.[1−5] Not only does TOF-SIMS provide information about the top few monolayers of the surface but it can also be used to generate a chemical image with submicrometer lateral resolution at the polymer surface.[6,7] While TOF-SIMS provides a glimpse of the composition of a surface, it is still a major challenge for TOF-SIMS analysis to overcome the low secondary ion yield in the high-mass region of the spectrum.

Different methods have been developed to improve upon the yield in this region.[4−6] Polyatomic primary ions have been found to increase total secondary ion yield. For example, a C_{60}^+ source has recently been shown to greatly enhance the TOF-SIMS signal of biological and polymer samples.[4,5,8] Laser postionization has been used to ionize neutrals formed during the sputtering process

to increase total possible ions, which improve the characterization at the surface of the sample.[9] Low-energy electrons reduce sample charging, which increase the secondary ions evolving from the surface.[10] Finally, the inclusion of heavy metals during sample preparation (metallic substrate or metallic monolayer on the surface) also facilitates molecular ion desorption.[2,7,8]

The evaporation of a monolayer of Au or Ag onto the sample surface has been found to enhance the SIMS signal of the underlying polymer substrate molecular species in the fingerprint region and that of Au and Ag cationized polymer species.[11,12] Evaporated metal also improves the lateral resolution of a SIMS image.[11−14] Increased lateral resolution, particularly with a small image field of view allows better recognition of one area from another (i.e., a more contrast). Metal evaporation is extremely effective and versatile over a range of polymer samples. However, these evaporation experiments require a metal evaporation chamber and a method to determine the thickness of the evaporated layers, such as the use of a quartz crystal microbalance or a profilometer. The precise structure of the metal overlayer is also difficult to control.

Presented here is an alternate approach, metal nanoparticle deposition (MND), which increases TOF-SIMS secondary ion yields of polymer molecules by depositing metals using a simple method that can be performed outside of vacuum during sample preparation. This method involves exposing the sample surface to a solution of citrate-capped Ag or Au nanoparticles.[15−19] As the

* To whom correspondence should be addressed. E-mail: nxw@psu.edu.

(1) Burlingame, A. L.; Gaskell S. J.; Boyd R. K. *Anal. Chem.* **1996,** *68* (12), 599R−651R.

(2) Burlingame, A. L.; Boyd R. K.; Gaskell, S. J. *Anal. Chem.* **1998,** *70* (16), 647R−715R.

(3) Van Vaeck, L.; Adrianens A.; Gijbels, R. *Mass Spectrom. Rev.* **1999,** *18,* 1−47.

(4) Weibel, D.; Wong, S.; Lockyer, N.; Blenkinsopp, P.; Hill, R.; Vickerman, J. C. *Anal. Chem.* **2003,** *75* (7), 1754−1764.

(5) Wong, S. C. C.; Hill, R.; Blenkinsopp, P.; Lockyer, N. P.; Weibel, D. E.; Vickerman, J. C. *Appl. Surf. Sci.* **2003,** *203,* 219−222.

(6) Belu, A. M.; Yang, Z. P.; Aslami, R.; Chilkoti, A. *Anal. Chem.* **2001,** *73* (2), 143−150.

(7) Kailas, L.; Audinot, J. N.; Migeon, H. N.; Bertrand, P. *Appl. Surf. Sci.* **2004,** *231−2,* 289−295.

(8) Postawa, Z.; Czerwinski, B.; Szewczyk, M.; Smiley, E.; Winograd, N.; Garrison, B. *Anal. Chem.* **2003,** *75* (17), 4402−4407.

(9) Winograd, N. *Anal. Chem.* **1993,** *65* (14), 622A-629A.

(10) Gilmore, I. S.; Seah, M. P. *Appl. Surf. Sci.* **2003,** *203,* 600−604.

(11) Delcorte, A.; Medard, N.; Bertrand, P. *Anal. Chem.* **2002,** *74* (19), 4955−4968.

(12) Delcorte, A.; Bour, J.; Aubriet, F.; Muller, J.-F.; Bertrand, P. *Anal. Chem.* **2003,** *75* (24), 6875−6885.

(13) Verlinden, G.; Gijbels, R.; Geuens, I.; De Keyzer, R. *J. Anal. At. Spectrom.* **1999,** *14* (3), 429−434.

(14) Verlinden, G.; Gijbels, R.; Geuens, I. Photographic Materials. In *ToF-SIMS: Surface Analysis by Mass Spectrometry*; Vickerman, J. C., Briggs, D., Eds.; Surface Spectra Limited; IM Publications: Manchester, U.K., 2001; pp 727−752.

(15) Adriaensen, L.; Vangaever, F.; Gijbels, R. *Anal. Chem.* **2004,** *76* (22), 6777−6785.

(16) Adriaensen, L.; Vangaever, F.; Lenaerts, J.; Gijbels, R. *Rapid Commun. Mass Spectrom.* **2005,** *19* (8), 1017−1024.

(17) Freeman, G. R.; Grabar, K. C.; Allison, K. J.; Bright, R. M.; Davis, J. A.; Guthrie, A. P.; Hommer, M. B.; Jackson, M. A.; Smith, P. C.; Walter, D. G.; Natan, M. J. *Science* **1995,** *276,* 1629−1632.

(18) Freeman, G. R.; Hommer, M. B.; Grabar, K. C.; Jackson, M. A.; Natan, M. J. *J. Phys. Chem.* **1996,** *100* (2), 718−724.

(19) Grabar, K. C.; Freeman R. G.; Hommer M. B.; Natan M. J. *Anal. Chem.* **1995,** *67,* 735−743.

polymer incorporates a submonolayer amount of the particles at the surface, the TOF-SIMS signals become significantly enhanced, with the spectra approaching those observed for monolayer films adsorbed onto the respective metal substrate. Au and Ag nanoparticles were chosen because these metals have been found to give signal enhancement in SIMS.

We utilize poly(tetrafluoroethylene) (PTFE) and polystyrene-g-poly(ethylene glycol) (Tentagel) as prototypical examples to illustrate the capabilities of this method. The PTFE sample, prepared as a thin film on Ag and as a bulk material, is important since the molecular ions are emitted without protonation. The Tentagel sample, prepared in the form of a spherical bead, represents a graft of two different polymers that exhibit protonated molecular ions. The results show that, for both Ag and Au MND, the mass range of the TOF-SIMS spectra of bulk polymers can be extended to 5000 Da and that the signal intensities are at least comparable to those found using metal deposition protocols. Moreover, since the coverage of particles is fairly low, high-mass imaging becomes feasible. We speculate that the mechanism of the enhancement is related to the unique collision cascade of moving atoms inside the metal nanoparticle and the opportunity of sputtered metal ions to cationize the desorbed polymer units.

MATERIALS AND METHODS

Materials. Three different polymers were employed in these experiments: Tentagel beads (Rapp-Polymere), bulk PTFE (Dupont et Nemours), and $HOC(CO_2Na)(CH_2CO_2Na)_2 \cdot 2H_2O]$, H_2O_2, and PTFE suspension (Aldrich Catalog No. 445096). Silicon substrates were piranha etched (3:1 H_2SO_4/H_2O_2) for 30 s to remove organic contaminants from the surface. Water used in sample preparation was purified using a Milli-Q system (Millipore, Burlington, MA) with a final resistivity of 18.2 MΩ cm.

Thin-Film Preparation. Silver foil was etched in concentrated HNO_3 for 10 s, rinsed in 18-MΩ water and then blown dry with N_2 (g) in preparation for casting of a thin film of PTFE. The diluted PTFE colloid was suspended in H_2O with a concentration of 15 mg/mL. A 65-μL aliquot of this diluted colloidal suspension was spin-cast at 3000 rpm for 30 s onto the etched Ag foil to form a film thin enough to allow for detection of Ag^+ ions.

Nanoparticle Synthesis. The nanoparticle synthesis apparatus consists of an aqua regia (3:1 concentrated HCl/HNO_3) cleaned 1000-mL two-neck round-bottom flask with a Kimble-Kontes coiled condenser and a football-shaped magnetic stirrer. This setup was placed in the appropriate heating mantle over a stirring plate. While the reactions were running, the second neck was closed off using a glass stopper. Au nanoparticles were synthesized using the Natan method.[17−19] The Ag nanoparticle synthesis was performed using 450 mL of 0.001 M $AgNO_3$ with 50 mL of 0.035 M $HOC(CO_2Na)(CH_2CO_2Na)_2 \cdot 2H_2O$. This solution was heated to reflux and allowed to react for 70 min. The Ag nanoparticles were allowed to cool for 1 h. The Au (6−12 nm) and Ag colloids (20−50 nm) were stored in Teflon-capped tinted glass bottles and refrigerated for future use.

MND on PTFE. Bulk PTFE was prepared by slicing an unexposed section of polymer from a piece of bulk sample. These samples were then rinsed with H_2O, inserted into a 2-mL solution of metal colloid, and allowed to stand for at least 24 h before analysis.

MND on Tentagel Beads. The Tentagel beads were immersed in a 10-mL solution of colloid in a chemical fume. Optimal exposure time is 2−3 days, although this time may be shortened by heating beads to boiling for 1 h.[21−24] Ag nanoparticle treated beads were allowed to react with the Ag nanoparticles for 24 h. Beads were isolated from solution by removing excess nanoparticles using pipet filtration and by drying for 24 h in a desiccator. Tentagel beads were placed on Si using glass pipets.

TOF-SIMS Measurements. The TOF-SIMS instrument used in these studies is described in detail elsewhere.[25] A pulsed 15-keV Ga^+ ion beam with a beam current between 1 and 2 nA, spot size of 100 nm, and a pulse width of 40 ns impinges the sample at 3 kHz causing secondary ions to desorb. These ions were collected using a time to digital converter with a time resolution of 2 ns. The ion fluence was kept below the static limit at less than 1.0×10^{12} ions/cm^2. Charge compensation was not required for these experiments. TOF-SIMS images were taken by rastering the beam over an area of 500 μm × 500 μm using 256 pixels × 256 pixels with 21 shots/pixel. Spectra were binned at 20 ns after acquisition for better visibility of weak molecular features. The ion currents were kept between 1 and 2 nA.

Scanning Electron Microscopy (SEM). SEM was performed on a JEOL 6700F field emitting scanning electron microscope (FE-SEM, University Park, PA). The magnification used was 80000×. The voltage used for analysis of the samples was 5.0 keV. The analysis area was 1.3 μm × 1.5 μm.

Coverage of Sample Surfaces from Metal Nanoparticle Deposition. One crucial issue inherent to the MND sample preparation of bulk polymers is the sample coverage of these particles. The coverage is dependent upon the type of metal nanoparticle and the polymer to be examined as well as the time of exposure to the nanoparticles: the shorter the exposure to the nanoparticle solution, the lower the surface coverage. The Ag MND samples typically exhibit a coverage of 85−90% whereas Au MND samples exhibit a coverage of ∼50%. The sizes of the nanoparticles were determined directly by high-resolution SEM as shown in Figure 1. Ag nanoparticles were found to be between 20 and 50 nm in size. Au nanoparticle islands are between 5 and 20 nm in size. The difference in coverage of Ag and Au nanoparticles may be one reason a larger signal enhancement is found for Ag nanoparticles versus Au nanoparticles.

Secondary Ion Yield and Yield Enhancement. Enhancement was calculated using the method reported by Delcorte.[12] Briefly, enhancement was calculated from the measured protonated molecular ion yield for a MND sample divided by the intensity of the same peak obtained from an untreated sample. The enhancement due to metal cationization was calculated similarly whereby the metal cationized molecule yield was divided by the untreated sample protonated ion yield. There is not a

(20) Burda, C.; Chen, X.; Narayanan, R.; El-Sayed, M. A. *Chem. Rev.* **2005**, *105*, 1025−1102.

(21) Enustun, B. V.; Turkevich, J. *J. Am. Chem. Soc.* **1963**, *85* (21), 3317−3328.

(22) Loginov, A. V.; Gorbunova, V. V.; Boitsova, T. B. *J. Nanopart. Res.* **2002**, *4* (3), 193−205.

(23) Satoh, N.; Hasegawa H.; Tsujii K.; Kimura K. *J. Phys. Chem.* **1994**, *98* (8), 2143−2147.

(24) Spear, E. B.; Jones P. F.; Neave A. S.; Shlager M. *J. Am. Chem. Soc.* **1921**, *43* (7), 1385−1391.

(25) Braun, R. M.; Blenkinsopp, P.; Mullock, S. J.; Corlett, C.; Willey, K. F.; Vickerman, J. C.; Winograd, N. *Rapid Commun. Mass Spectrom.* **1998**, *12* (18), 1246−1252.
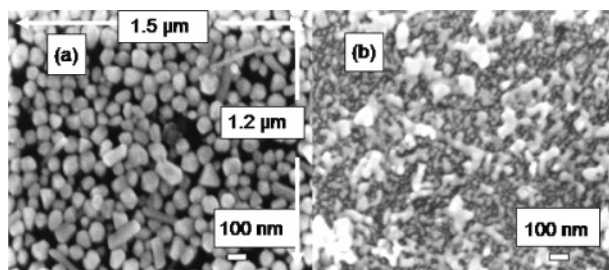
Figure 1. (a) SEM of Ag nanoparticle treated Tentagel bead surface. (b) SEM of Au nanoparticle treated Tentagel bead surface (the darker fine grain materials). The Ag treated bead surface has far greater coverage than that of the Au treated sample.
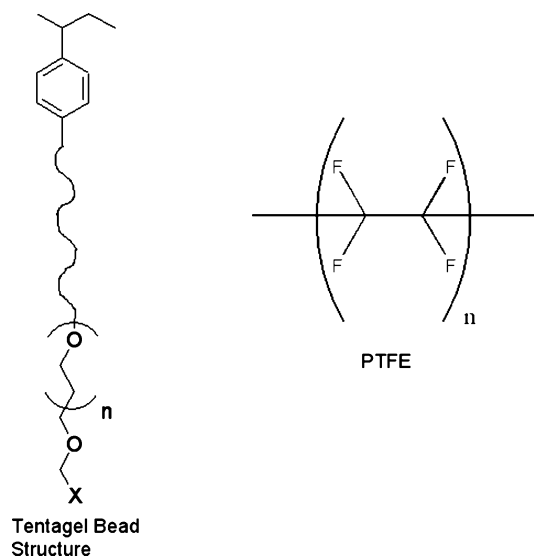

Figure 2. Molecular structures of Tentagel beads and PTFE.

Figure 3. The 0−200 Da region of thin-film colloidal PTFE on etched Ag. The fingerprint of ions for the PTFE are the following: C^+ (m/z 12), CF^+ (m/z 31), CF_3^+ (m/z 69), $(CF_2)_2^+$ (m/z 100), $(CF_2)_2CF^+$ (m/z 131), $(CF_2)_3^+$ (m/z 150), $(CF_2)_2CF_3^+$ (m/z 169), and $C_4F_7^+$ (m/z 181).

Figure 4. TOF-SIMS spectrum of thin-film PTFE on etched Ag foil. Mass spectrum of MND PTFE with a range of 0−3000 Da. The low-mass range from 0 to 200 is considered to be the fingerprint region. The $[C_2(CF_2)_7C_3F + (C_2F)]^+$ ions are marked with orange asterisks to guide the eye. The less abundant $[C_2(CF_2)_7C_3FO + (C_2F)]^+$ oligomer series are marked with purple asterisks to mark these particular ions. The $[(CF_2)_{20}CAg + (C_2F)_n]^+$ ions are marked with pink asterisks to guide the eye to the proper ions in this series. The $[(CF_2)_{24} + (C_2F)_n]^+$ ions are marked with light blue asterisks to guide the eye to the proper ions.

homologue metal cationized peak in the pristine sample, so the only peak that can be used to determine the degree of enhancement is the protonated ion yield. M^+ indicates the molecular fragment ion whereas Me^+ indicates the metal ion. Total yield enhancement is defined as being equal to the protonated ion yield enhancement plus the metal cationized ion yield enhancement.

RESULTS AND DISCUSSION

The effectiveness of MND signal enhancement was examined on two different polymer systems: poly(tetrafluoroethylene) (PTFE) and polystyrene-*g*-poly(ethylene glycol) (Tentagel) (Figure 2). The PTFE samples show that there is signal enhancement using MND on the PTFE polymer from detection of the molecular or oligomer ion (M^+). The Tentagel bead sample shows a similar signal enhancement using MND with protonation $[M + H]^+$ and metal cationization $[M + Me]^+$ ionization mechanisms.

The samples to be examined are thin-film PTFE on etched Ag, bulk PTFE, and Tentagel beads. Several characteristic mass peaks are singled out for attention. For the thin-film PTFE film sample, there is a strong fragment ion peak $[(CF_2)_{32}CF]^+$ at m/z 1631. Bulk PTFE exhibits the same high-mass peak. In either case, PTFE does not ionize through a protonation mechanism, but forms a radical cation directly. For Tentagel beads there is a characteristic ion $[O(CH_2CH_2O)_{28}(C_6H_4CH_2CH_2O_2H)_7 + H]^+$ at m/z 2209, while corresponding metal cationized peaks are observed at m/z 2315, 2317 $[Ag + O(CH_2CH_2O)_{28}(C_6H_4CH_2CH_2O_2H)_7]^+$ or m/z
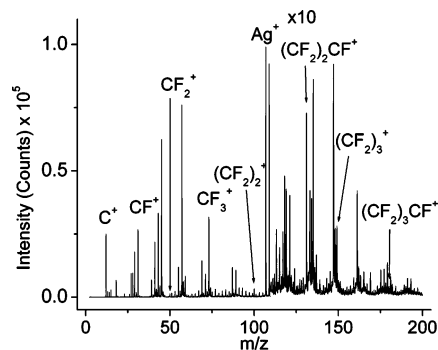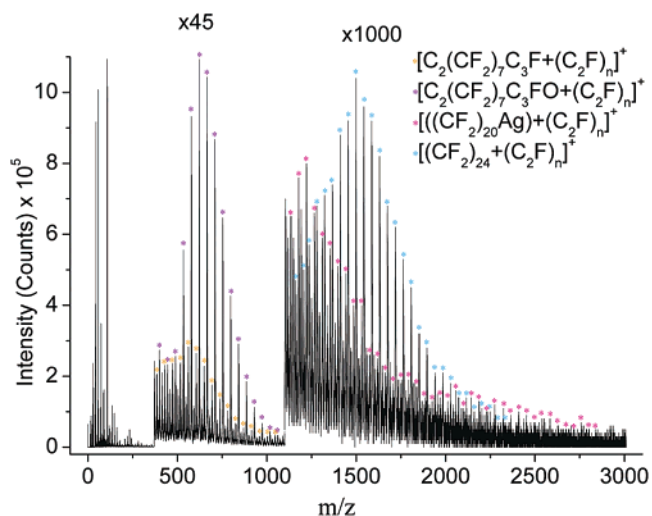
2405 $[Au + O(CH_2CH_2O)_{28}(C_6H_4CH_2CH_2O_2H)_7]^+$. In the low-mass range, $[(CH_2CH_2O)_2]^+$ and $[(CH_2CH_2O)_2 + H]^+$ with a m/z 88 and 89, respectively, are chosen as representative peaks. In the case of all ions, the metalated ion has a higher intensity than the molecular or protonated ion.

Thin-Film PTFE Control Sample. The control PTFE thin film on etched Ag exhibits several regions of interest. The low-mass region from m/z 0 to 200, or the fingerprint region, has a characteristic distribution of representative low-mass ions, which allow identification of the PTFE as shown in Figure 3. The higher mass range is shown in Figure 4 and consists of two peak distributions of m/z 475−955, $[C_2(CF_2)_7C_3F + (C_2F)_n]^+$, and m/z 487−912, $[C_2(CF_2)_7C_3FO + (C_2F)_n]^+$. These two oligomer ion series are related in structure since series $[C_2(CF_2)_7C_3FO + (C_2F)_n]^+$ has an shift of 16 mass units from the series $[C_2(CF_2)_7C_3F + (C_2F)_n]^+$. This observation indicates that the surface of the polymer is at least partially oxidized. The last part of the mass spectrum consists of two series polymer ion fragments from m/z
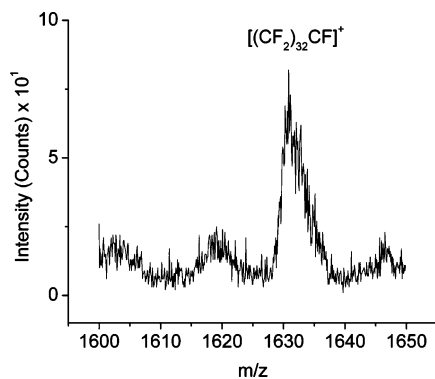
Figure 5. $[(CF_2)_{32}C_2F]^+$ formation off etched Ag foil. There is considerable ion formation at this high mass.

1131 to 2581 $[(CF_2)_{20}CAg + (C_2F)_n]^+$ and from m/z 1174 to 2674 $[(CF_2)_{24} + (C_2F)_n]^+$.

Metal cationization and oligomer ion formation of PTFE molecular ion signals occurs using the etched Ag foil. Some ions formed have metal conjugate ions, which facilitate their production and evolution from the analyzed surface. In the high-mass region, the molecular ion fragment $[(CF_2)_{32}CF]^+$ with m/z 1631 is observed as shown in Figure 5. The metal cationized oligomer ion, however, is not detected for this oligomer ion series.[26,27] Presumably, a metastable decay of the metal cationized ion into the charged m/z 1631 ion and a neutral Ag atom is responsible for this observation.[28−31]

Positive Ion Signal Enhancement of Bulk PTFE Using MND. Addition of Au or Ag MND on bulk PTFE yields TOF-SIMS spectra that are similar in intensity at high mass to the spectrum observed for thin-film PTFE on etched Ag foil. The mass spectrum of the untreated bulk PTFE is shown in Figure 6a. This untreated PTFE sample does not exhibit measurable signal in the mass range from m/z 1250 to 3000. The Au and Ag MND bulk PTFE mass spectra are shown in Figure 6b and c. The mass spectra in Figures 4, 6b, and 6c illustrate an analogous degree of enhancement at high mass in the region of m/z 1250−3000 between the thin-film PTFE sample and the MND PTFE treated samples. Both sample types give significant oligomer ion formation (Figures 4, 6b, and 6c). The characteristic oligomer fragments for the thin-film PTFE are $[(CF_2)_{20}CAg + (C_2F)_n]^+$ and $[(CF_2)_{24} + (C_2F)_n]^+$ from m/z 1250 to 3000 as shown in Figure 4. The characteristic oligomer ions for MND treated bulk PTFE are $[(CF_2)_nC_2F]^+$, $[(CF_2)_nCF]^+$, and $[(CF_2)_nC_2]^+$, which are illustrated in Figure 6b (PTFE−Au MND) and Figure 6c (PTFE−Ag MND). While the high-mass spectra of the thin-film PTFE and the bulk PTFE are different, the increase in the formation of secondary oligomer ions is similar. The mass spectra differ at high mass
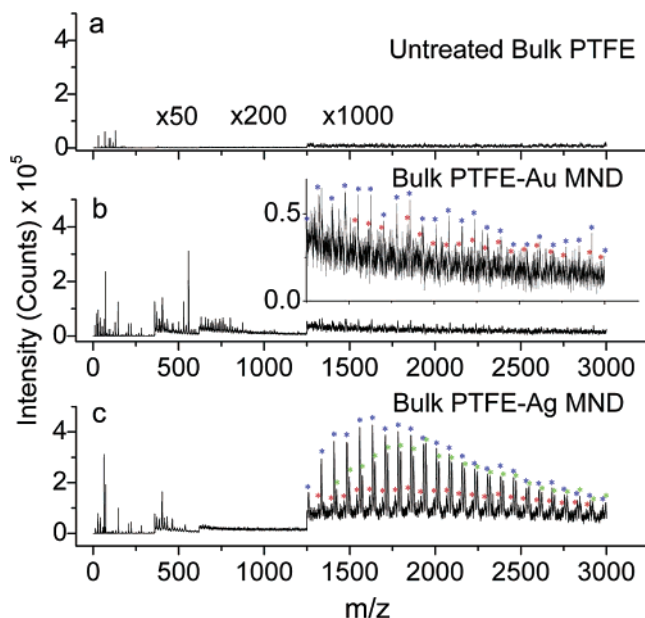
(26) Gamble, L. J.; Ravel, B.; Fischer, D. A.; Castner, D. G. *Langmuir* **2002**, *18* (6), 2183−2189.

(27) Hagenoff, B. Optimisation Methods: Cationisation. In *ToF−SIMS: Surface Analysis by Mass Spectrometry*, 1 ed.; Vickerman, J. C., Briggs, D., Eds.; IM Publications and Surface Spectra: Charlton, Chichester, West Sussex, 2001; pp 285−308.

(28) Bletsos, I. V.; Hercules, D. M.; vanLeyen, D.; Benninghoven, A. *Macromolecules* **1987**, *20* (2), 407−413.

(29) Bletsos, I. V.; Hercules, D. M.; Magill, J. H.; vanLeyen, D.; Niehuis, E.; Benninghoven, A. *Anal. Chem.* **1988**, *60* (9), 938−944.

(30) Bletsos, I. V.; Hercules, D. M.; vanLeyen, D.; Benninghoven, A.; Karakatsanis, C. G.; Rieck, J. N. *Macromolecules* **1990**, *23* (18), 4157−4163.

(31) Bletsos, I. V.; Hercules, D. M. *Anal. Chem.* **1991**, *63* (18), 1953−1960.

Figure 6. Mass spectra of MND bulk PTFE with a range of 0−3000 Da. (a) Untreated bulk PTFE. (b) Au nanoparticle treated bulk PTFE. The inset spectrum is the high-mass region expanded to illustrate the formation of the characteristic high-mass oligomer ions. The $(CF_2)_nCF^+$ ions are marked with blue asterisks to guide the eye to the proper range. The less abundant $(CF_2)_nC_2^+$ oligomer series are marked with a red asterisks to mark the specific peaks of this particular ion series. (c) Ag nanoparticle treated bulk PTFE. The $(CF_2)_nCF^+$ ions are marked with blue asterisks to guide the eye to the proper range. The less abundant $(CF_2)_nC_2^+$ oligomer series are marked with a red asterisks to mark the specific peaks of this particular ion series. The $(CF_2)_nC_2F^+$ ions are marked with green asterisks to guide the eye to the proper range. The $(CF_2)_nC_2^+$ series is marked with a red line to guide the eye to the proper range.

since the bulk PTFE is sintered and molded, enabling a cross-linking reaction between the chains of the PTFE grains and the molecular weight is probably higher.[32−34]

It is interesting to examine the intensity of a few key high-mass ions when the MND is placed upon the bulk PTFE surface. One ion with structure $[(CF_2)_nCF]^+$ with $n = 32$ at m/z 1631 is not observed unless the sample is treated with Ag or Au nanoparticles or unless a thin film of PTFE is prepared on an etched Ag substrate. Ths ion was chosen for examination since it is one of the most intense peaks in the Ag MND and Au MND spectra as well as being a characteristic oligomer ion for the bulk PTFE and the thin-film PTFE sample. Increased signal from the Ag and Au MND sample at m/z 1631 is observed and shown in Figure 7a and b, respectively. The $[(CF_2)_{32}CF]^+$ ion exhibits 22- and 160-fold enhancement with Au and Ag treatment, respectively. Ions formed from the Ag nanoparticle treated surfaces are 5−6 times more abundant than their Au ion counterparts as demonstrated in Table 1. In addition, as shown in Figure 5 and Figure 7a, there are more secondary ions formed using Ag MND than that of thin-film PTFE on etched Ag foil. Au MND PTFE has a secondary ion intensity equivalent to that of the thin-film PTFE on etched Ag foil for the $[(CF_2)_{32}CF]^+$ ion as seen in Figure 5 and Figure 7b.

(32) E. I.du Pont de Nemours & Co. US 2965565, 1958.

(33) Fields, R. T. US 2456262, 1948.

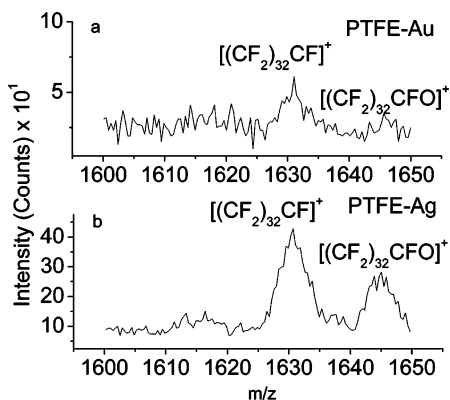(34) Venkateswarlu, P.; Kolb, R. E.; Guethner, R. A. *Polym. Prepr.* **1989**, *31* (1), 360−361.

Figure 7. (a) Au nanoparticle treated PTFE at $[(CF_2)_{32}CF]^+$. (b) Ag nanoparticle treated PTFE at $[(CF_2)_{32}CF]^+$. Au and Ag nanoparticle treated samples have distinct peaks at $[(CF_2)_{32}CF]^+$ In addition to M^+, $[M + H]^+$ and $[M + 2H]^+$ also occur as is evident from the spectra in (a) and (b) due to the width of the peaks.

Table 1. Secondary Ion Yields (Y, 10^2 Counts/nC) and Enhancements (E) Measured for Tentagel and Bulk PTFE

sample			untreated	nano-particle Au	nano-particle Ag
bulk PTFE $[(CF_2)_{32}CF]^+$					
	M	Y	not obsd	290	2000
		E	1	22	160
	$M + Me^a$	Y	n/a	31	200
		E	n/a	2	15
		tot enhanc^b	1	24	175
Tentagel $[O(CH_2CH_2O)_{28}$-$(C_6H_4CH_2CH_2O_2H)_7]^+$					
	$M + H$	Y	1.1	38	54
		E	1	33	48
	$M + Me^a$	Y	n/a	86	430
		E	n/a	76	380
		tot enhanc^b	1	109	428
Tentagel $[(CH_2CH_2O)_2]^+$					
	$M + H$	Y	1100	2900	4600
		E	1	3	4
	$M + Me^a$	Y	n/a	1900	9000
		E	n/a	2	8
		tot enhanc^b	1	5	12

^{a} All enhancements are calculated by enhancement untreated is yield untreated/yield untreated ($E = Y_{Untreated}/Y_{Untreated}$) while enhancement treated is yield nanoparticle treated sample/yield untreated ($E = Y_{Untreated}/Y_{Treated}$). The metal cationized enhancement (+Me) calculations were calculated from the yield of the metal cationized peak over the yield of the untreated peak since the metal cationized peak for the peak will not occur on the untreated sample. ^{b} Total enhancement.

It is possible to take advantage of the MND methodology to acquire molecule-specific images of the polymer surface as shown in Figure 8. Each sample shows areas of varied intensity and roughness due predominantly to the polymer topography. The untreated sample exhibits differences in intensity due to surface roughness and lower secondary ion formation as illustrated in Figure 8a−d. The Au and Ag MND samples exhibit differences in intensity due to topological effects as well. These effects are shown in Figure 8h and m, where the images represent the intensity variation of the respective metal ion as a result of differences in height of the polymer roughness. The topography
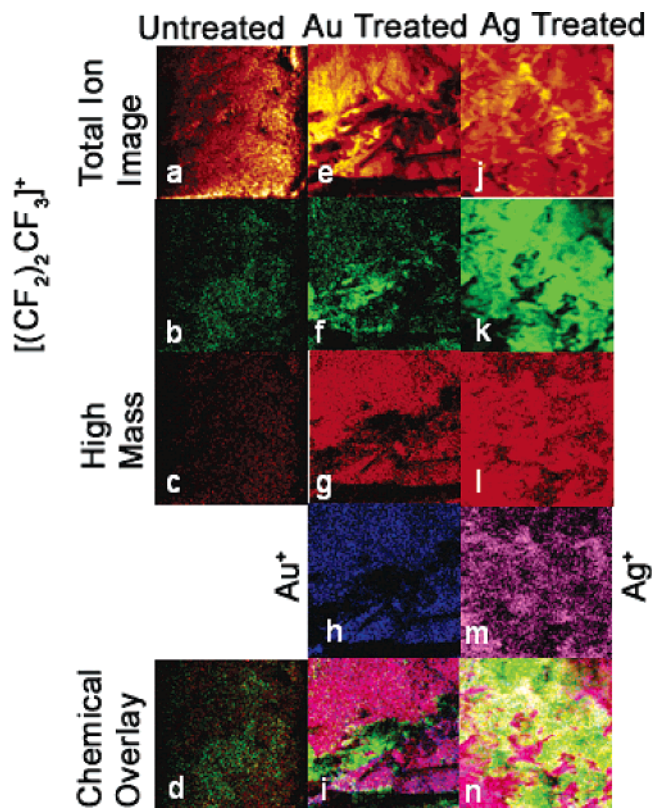

Figure 8. (a) Total ion image from bulk PTFE. (b) Chemical ion image of 169 Da $[((CF_2)_2)CF_3]^+$. (c) 1100−3200 Da chemical image from untreated bulk PTFE. (d) Chemical overlay of 169 Da $[((CF_2)_2)$-$CF_3]^+]$ and 1100−3200 Da molecular image from pristine bulk Au nanoparticle treated PTFE. (e) Total ion image from Au NMD bulk PTFE. (f) Chemical image of bulk PTFE $[((CF_2)_2)CF_3]^+$ peak. (g) Chemical image of Au bulk PTFE from 1100 to 3200 Da. (h) Chemical image of Ag^+ from bulk PTFE. (i) Overlay of chemical images from bulk PTFE of Ag^+, $[(CF_2)_2)CF_3]^+$, and high mass. (j) Total ion image from Ag NMD bulk PTFE. (k) Chemical image of bulk PTFE $[((CF_2)_2)$-$CF_3]^+$ peak. (l) Chemical image of Ag treated bulk PTFE 1100−3200 Da. (m) Chemical image of Ag^+ from bulk PTFE. (n) Overlay of chemical images from bulk PTFE of Ag^+, $[((CF_2)_2)CF_3]^+$, and 1100−3200 Da range of the Ag nanoparticle treated bulk PTFE.

of the surfaces arise from the blade used to cut the samples which cause the total ion intensity variations seen in Figure 8e and j.

Low-mass ions are formed where there is low metal ion signal. The highest intensity for the low-mass fragments, $[(CF_2)_2CF_3]^+$ for Au and Ag treated PTFE (Figure 8f, k) coincides with the lowest intensity for the metal nanoparticle coverage (Figure 8h, m), respectively. This result implies that the lower the metal nanoparticle coverage, the higher the low-mass fragmentation will be from the polymer oligomers which evolve during the collision cascade.

For the MND treated samples, the high-mass fragments colocalize with high the metal ion signal. The untreated bulk PTFE at high mass exhibits significantly lower intensity when compared to the MND treated samples. The red high-mass peak images (m/z 1100−3200 range, Figure 8g, l) do colocalize with the blue metal ion images (Figure 8h, m). The higher the metal nanoparticle coverage (Figure 8h, m), the greater the high-mass oligomer detection will be up to a point, of course. The MND sample preparation allows images of ion mappings to be acquired for bulk polymer surfaces. The uniformity of the metal nanoparticles is
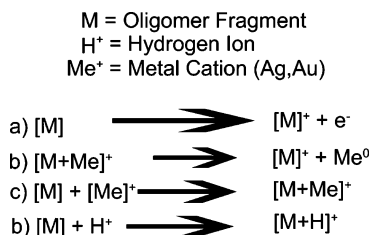
M = Oligomer Fragment
H⁺ = Hydrogen Ion
Me⁺ = Metal Cation (Ag,Au)

a) [M] $\longrightarrow$ [M]⁺ + e⁻

b) [M+Me]⁺ $\longrightarrow$ [M]⁺ + Me⁰

c) [M] + [Me]⁺ $\longrightarrow$ [M+Me]⁺

b) [M] + H⁺ $\longrightarrow$ [M+H]⁺

Figure 9. Ionization mechanisms during for increased secondary ion yields. (a) A neutral polymer fragment, which loses an electron to form a positively charged polymer ion. (b) An ionized metal–polymer fragment pair formed during the collision cascade, which undergoes a metastable decay into an ion and a neutral metal atom (c) A neutral polymer fragment collides with a metal cation to form a metal cationized polymer fragment ion. (d) Metal cationization due to a reaction between a neutral polymer fragment and a proton. This reaction could occur in the gas phase or at the surface of the metal nanoparticle.

shown by the SEM images in Figure 1. These images are 1 μm whereas the TOF-SIMS images are 500 μm. This coverage is seen as a uniform coverage with a TOF-SIMS imaging experiment.

MND enhancement of PTFE can occur by two main pathways: (1) the loss of an electron to form a free radical positively charged oligomer ion or (2) oligomer formation via metal cationization of the PTFE molecule followed by a metastable decay. A possible mechanism for oligomer ion formation is through the loss of an electron to form the ion from the neutral fragment to form the charged oligomer ion (Figure 9a). Oligomer ion formation in MND treated bulk PTFE occurs presumably from a metal–oligomer conjugate ion (formed through metal cationization, Figure 9b), which undergoes metastable decay into an oligomer ion and a neutral metal atom (Figure 9c).[28–31] Figure 9d shows oligomer ion enhancement through a reaction with a proton. This mechanism is not applicable to the PTFE polymer since this polymer does not have any available hydrogen in its molecular structure.

Positive Ion Signal Enhancement of Tentagel Beads Using MND. An application of MND for bulk polymer samples is the examination of Tentagel beads using Au and Ag nanoparticles. The most striking difference between the untreated sample and the MND treated Au and Ag treated Tentagel beads occur in the mass range from m/z 500 to 4000 as shown in Figures 10a and 11a. There is significant ion formation in the mass range from m/z 500 to 1600 in the MND samples with oligomers of the form $[((CH_2)_2O)_n + Na]^+$ and $[((CH_2)_2O)_n + CH_2Na]^+$ for both the Au and Ag treated samples as shown in Figures 10b and 11b for Tentagel–Au and Figures 10c and 11c for Tentagel–Ag. The $[((CH_2)_2O)_n + (CH_2)_2Na]^+$ oligomer ion series is only present in the Au treated sample whereas the Ag MND sample exhibits the characteristic polymer fragment series $[((CH_2)_2O)_n + CH_2ONa]^+$ (Figure 11b, c). In the m/z range of 1600–4000, the MND samples exhibit ions cationized with either Ag or Au. The $[((CH_2)_2)_{40}OCH_2Au + (C_6H_4(CH_2)_2O_2H)_n]^+$ occurs in the Au MND Tentagel sample (Figure 10b). The Ag MND sample exhibits two high-mass oligomer ion series: $[((CH_2)_2)_{28}OAg + (C_6H_4(CH_2)_2O_2H)_n]^+$ and $[((CH_2)_2O)_{28}AgNaHO_2(CH_2)_2 + (C_6H_4O_2(CH_2)_2H)_n]^+$ (Figure 10c).

It is instructive to select a few characteristic ions from the Tentagel beads to examine the degree of enhancement at high
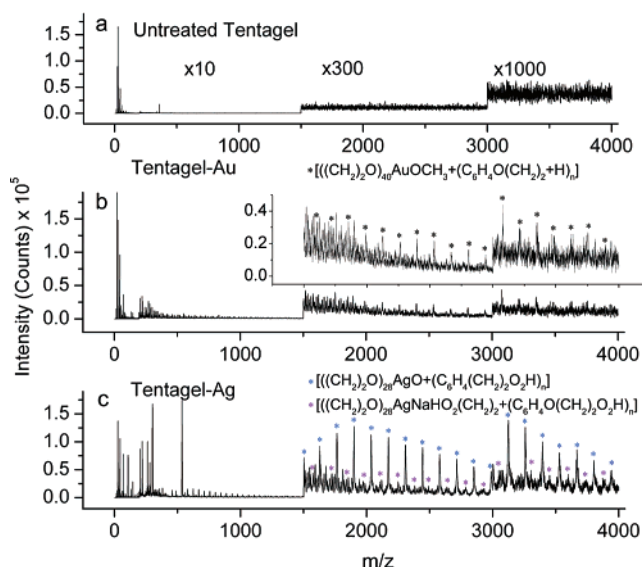

Figure 10. Mass spectra of MND and untreated Tentagel beads from 0 to 4000 Da. Full spectra for Tentagel beads: (a) untreated; (b) Au MND Tentagel; (c) Ag-MND Tentagel. The fingerprint region is from m/z 0 to 200. Significant oligomer ion formation occurs in two regions: 500–1600 and 1600–4000 Da. The oligomer ions formed from 1600 to 4000 Da are $[((CH_2)_2)_{40}OCH_2Au + (C_6H_4(CH_2)_2O_2H)_n]^+$ for the Au MND treated sample and $[((CH_2)_2)_{28}OAg + (C_6H_4-(CH_2)_2O_2H)_n]^+$ and $[((CH_2)_2O)_{28}AgNaHO_2(CH_2)_2 + (C_6H_4O_2(CH_2)_2H)_n]^+$ for the Ag MND treated sample.
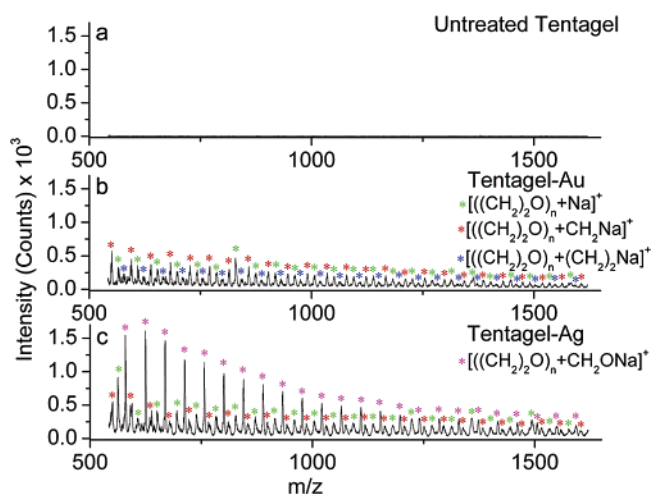

Figure 11. Untreated Tentagel from m/z 500 to 1600. (a) The spectrum for the untreated control. (b) Au MND Tentagel from m/z 500 to 1600. There are three characteristic oligomer ion series: $[((CH_2)_2O)_n+Na]^+$, $[((CH_2)_2O)_n + CH_2Na]^+$, and $[((CH_2)_2O)_n + (CH_2)_2-Na]^+$. (c) Ag MND Tentagel from m/z 500 to 1600. There are three characteristic oligomer ion series: $[((CH_2)_2O)_n + Na]^+$, $[((CH_2)_2O)_n + CH_2Na]^+$, and $[((CH_2)_2O + CH_2ONa]^+$.

mass due to MND treatment. An abundant, characteristic ion for examination is at m/z 2209 $[O(CH_2CH_2O)_{28}(C_6H_4CH_2CH_2O_2H)_7 + H]^+$ and the metalated homologues m/z 2405 $[AuO(CH_2-CH_2O)_{28}(C_6H_4CH_2CH_2O_2H)_7]^+$ and m/z 2315 and 2317 $[AgO(CH_2-CH_2O)_{28}(C_6H_4CH_2CH_2O_2H)_7]^+$ associated with this high-mass peak. The untreated sample does not exhibit a peak at m/z 2209 (Figure 12a). There is significant signal for the high-mass oligomer ion plus a proton at m/z 2209 for the Au and Ag MND treated Tentagel beads. The m/z 2209 peak is clearly seen in the Au and Ag MND Tentagel bead spectra (Figure 12b, c). The enhancement
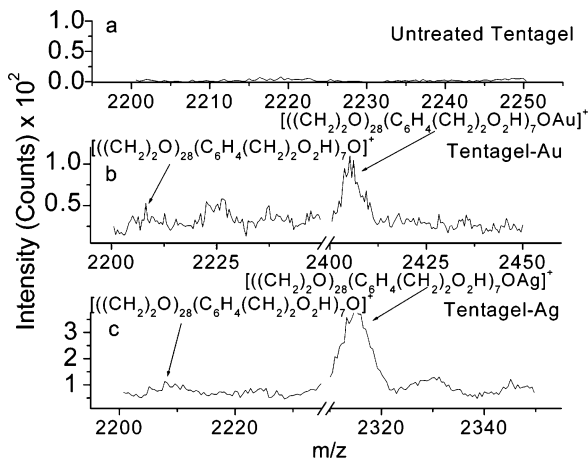
Figure 12. (a) Pristine Tentagel bead signal at high mass [(CH$_2$CH$_2$O)$_{50}$ + H]. (b) Au nanoparticle treated Tentagel beads for [((CH$_2$)$_2$O$_{28}$(C$_6$H$_4$(CH$_2$)$_2$O$_2$H)$_7$O]$^+$ and [((CH$_2$)$_2$O$_{28}$(C$_6$H$_4$(CH$_2$)$_2$O$_2$H)$_7$O]$^+$ + Au]$^+$. (c) Au nanoparticle treated Tentagel beads for [((CH$_2$)$_2$O$_{28}$(C$_6$H$_4$(CH$_2$)$_2$O$_2$H)$_7$O]$^+$ and [((CH$_2$)$_2$O$_{28}$(C$_6$H$_4$(CH$_2$)$_2$O$_2$H)$_7$O + Ag]$^+$.
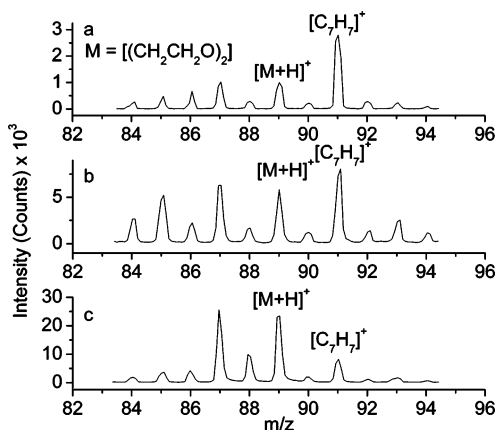
Figure 13. (a) Untreated low-mass region for the protonated dimer [(CH$_2$CH$_2$O)$_2$ + H]$^+$. (b) Au nanoparticle treated Tentagel low-mass dimer [(CH$_2$CH$_2$O)$_2$ + H]$^+$ region. Unlike the pristine bead, the signal is higher and even exceeds the styrene peak (91 Da), which was not the case in the pristine bead (a). (c) Ag nanoparticle treated Tentagel bead in the [(CH$_2$CH$_2$O)$_2$ + H]$^+$ region.

of the Au MND and Ag MND samples were 33 and 48 (Table 1). Other enhancement factors are noted in Table 1. While the emphasis of this paper deals with the larger secondary ion yields at high mass from polymer samples, there is also a small degree of signal enhancement noted at low mass for proton cationized species of Tentagel beads as shown in Figure 13.

The increased sensitivity using MND on a polymer improves molecular imaging of the polymer surface due to the increased protonated and metalated oligomer ions. The total ion images (Figure 14a, c, and g) show that the MND treatment results in higher secondary ion signal. The signal for the protonated Tentagel fragment, at m/z 2209, is clearly seen with MND (Figure 14d, h). This result means that the MND treatment enables the oligomer ion to be formed and retain stability during the course of the SIMS experiment. The metal ion signal is depicted with the blue chemical mappings (Figure 14f, j). The highest degree of protonated oligomer ion at m/z 2209 localizes to the most intense regions of the metal ion images.

Utilizing metal nanoparticles facilitates metal cationization of oligomer ions on Tentagel beads. Should the characteristic
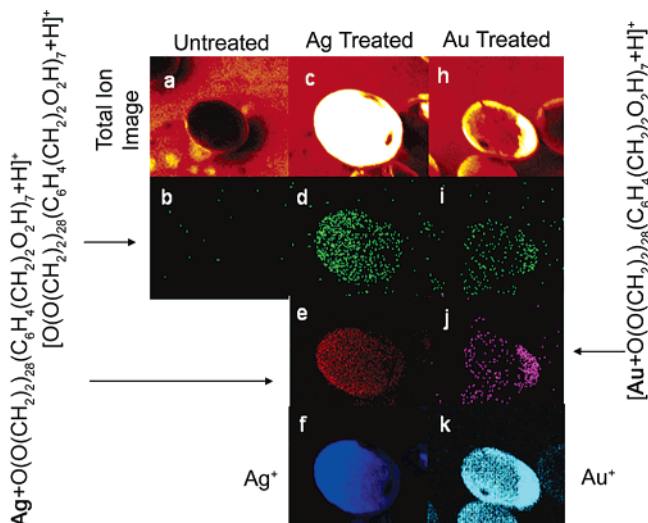

Figure 14. (a) Total ion image untreated Tentagel bead. (b) Chemical image of 2209 Da [O(CH$_2$CH$_2$O)$_{28}$(C$_6$H$_4$CH$_2$CH$_2$O$_2$H)$_7$ + H]$^+$. (c) Total ion image Ag NMD Tentagel bead. (d) 2209 Da [O(CH$_2$CH$_2$O)$_{28}$(C$_6$H$_4$CH$_2$CH$_2$O$_2$H)$_7$ + H]$^+$ chemical image from the bead. (e) 2315 Da [AgO(CH$_2$CH$_2$O)$_{28}$(C$_6$H$_4$CH$_2$CH$_2$O$_2$H)$_7$]$^+$ chemical image from NMD Tentagel bead. (f) Ag$^+$ chemical image from NMD Tentagel bead. (g) Total ion image of Au NMD Tentagel beads. (h) 2208 Da [O(CH$_2$CH$_2$O)$_{28}$(C$_6$H$_4$CH$_2$CH$_2$O$_2$H)$_7$ + H]$^+$. (i) 2405 Da [AuO(CH$_2$CH$_2$O)$_{28}$(C$_6$H$_4$CH$_2$CH$_2$O$_2$H)$_7$]$^+$ chemical image. (j) Au$^+$ chemical image from NMD Tentagel bead.

polymer fragment ion plus a proton peak not be present when using MND, the metalated characteristic fragments may be formed. For example, the MND Tentagel beads have metalated characteristic fragments at m/z 2315 [AgO(CH$_2$CH$_2$O)$_{28}$(C$_6$H$_4$CH$_2$CH$_2$O$_2$H)$_7$]$^+$ and m/z 2415 [AuO(CH$_2$CH$_2$O)$_{28}$(C$_6$H$_4$CH$_2$CH$_2$O$_2$H)$_7$]$^+$, as seen in Figure 14e and j. One interesting point is that the secondary ion formation for the metalated oligomer fragments colocalize with the most intense areas of the metal ion images (Figure 14e, f and i, j). The colocalization means that these high-mass ions form exclusively where the metal nanoparticles occur, suggesting that both the metal cationization and protonation are enhanced because of the presence of the nanoparticles.

Mechanisms of Positive Secondary Ion Enhancement. There is not yet a comprehensive theory to describe the mechanism behind the influence of MND on polymer surfaces. We presume that the phenomenon is very similar to that observed by Delcorte et al. with metal evaporation experiments.[11,12] His group proposed that cationized high-mass oligomer ions (2-kDa oligomers) originate from these high-mass molecules neighboring metal islands through improved or additional charge-transfer mechanisms.[12,35] In our case, similar dynamics undoubtedly takes place, although the uniformity of the size of the clusters offer some interesting ways to time the enhancement even further.[20,36]

Metal cationization plays a large role in signal enhancement from MND on bulk polymers. The Tentagel system exhibits M + Me$^+$ fragments from m/z 1250 to 3000 for the Au and Ag treated samples (Figure 9b). Unlike the Tentagel, the PTFE only shows the oligomer fragments, M$^+$. These oligomer ions may form from a metastable decay from M + Me$^+$ to M$^+$ (Figure 9c).

(35) Delcorte, A.; Garrison, B. J. *J. Phys. Chem. B* **2004**, *108* (40), 15652−15661.
(36) Ahmadi, T. S.; Zhong L. W.; Green T. C.; Henglein A.; El-Sayed M. A. *Science* **1996**, *272*, 1924−1926.

Increased secondary ion formation also occurs as a result of a loss of an electron from the polymer to the metal nanoparticle. The charged secondary ion radical formation forms from a donation of an electron from the polymer molecule to the metal nanoparticle.[37,38] The loss of one electron helps to stabilize the secondary PTFE oligomer ion facilitating its enhancement with MND (Figure 9d).

The protonation due to metal nanoparticle deposition can improve the secondary ion formation of the Tentagel polymer. Metal nanoparticles have been found to have protons adhering to their surfaces.[39] This abundance of hydrogen ions at the surface of the metal nanoparticles may allow increased ionization to occur during the collision cascade since this is an extra source of protons over those inherent hydrogen ions available in the bulk polymer. These hydrogen ions can be kicked into the gas phase during the collision cascade, enabling $M + H^+$ to be more readily formed (Figure 9c).

Negative Ion Signal Enhancement of PTFE and Tentagel Using MND. The negative ion SIMS spectra were investigated with TOF-SIMS for both PTFE and Tentagel beads. Examination of PTFE without metal nanoparticle deposition exhibits only low-mass fragments.[40] Addition of metal nanoparticles to the surface allows many strong oligomers to be detected due to increased secondary ion formation although anionization is not observed. For example, $[(CF_2)_nC_2F_4]^-$ oligomer ions are found to be enhanced with MND. The same trend also occurs in negative mode with Tentagel beads where the observed characteristic oligomer ions are $[(C_{16}H_{22}O_5)_nC_6H_5CH_2CH_2OCH_2CH_2O]^-$. The

degree of enhancement in negative mode for both PTFE and Tentagel is similar to that of the positive ion mode enhancement.

CONCLUSIONS

Utilizing MND, a simple ex vacuo technique, signal enhancement of high-mass oligomer ions from PTFE and Tentagel bulk polymers, has been achieved. Utilizing metal nanoparticles allows control of the size of the metal particles. This control in size and shape may allow a further signal enhancement for TOF-SIMS experiments. Greater intensities of secondary ions are formed with MND treatment over the secondary ion intensities from untreated samples. Increased sensitivity of SIMS images on bulk polymer surfaces are obtained through MND treatment on both PTFE and Tentagel. In the future, we hope to utilize MND to characterize a small combinatorial library on bead and to enable an examination of cells with focused ion beams.

(37) Chapman, R.; Mulvaney, P. *Chem. Phys. Lett.* **2001**, *349*, 358−362.
(38) Cury, L. A.; Ladeira, L. O.; Righi, A. *Synth. Met.* **2003**, *139*, 283−286.
(39) Buckart, S.; Gantefor, G.; Kim, Y. D.; Jena, P. *J. Am. Chem. Soc.* **2003**, *125* (46), 14205−14209.
(40) *The Static SIMS Library,* 1st ed.; John Wiley & Sons: New York, 1996; Vol. 2.